Journal of Optics

PURPOSE-LED PUBLISHING™

LETTER • OPEN ACCESS

Fuzzy reliability framework for optical phase unwrapping

To cite this article: Davood Khodadad and Satyam Paul 2026 *J. Opt.* **28** 08LT01

View the article online for updates and enhancements.

You may also like

- Multi task deep learning phase unwrapping method based on semantic segmentation
Linlin Wang, Wenjie Liang, Wanyi Guo et al.
- Robust phase unwrapping algorithm based on Zernike polynomial fitting and Swin-Transformer network
Zixin Zhao, Menghang Zhou, Yijun Du et al.
- Transformer based deep learning hybrid architecture for phase unwrapping
Karthik Goud Bujagouni and Swarupananda Pradhan

This content was downloaded from IP address 130.239.180.10 on 06/08/2026 at 14:17

Journal of Optics

Check for updates

OPEN ACCESS

RECEIVED
19 May 2026

REVISED
6 July 2026

ACCEPTED FOR PUBLICATION
24 July 2026

PUBLISHED
6 August 2026

Original content from this work may be used under the terms of the Creative Commons Attribution 4.0 licence.

Any further distribution of this work must maintain attribution to the author(s) and the title of the work, journal citation and DOI.

LETTER

Fuzzy reliability framework for optical phase unwrapping

Davood Khodadad[1,*] and **Satyam Paul**[2]

[1] Department of Applied Physics and Electronics, Umeå University, 90187 Umeå, Sweden
[2] School of Science and Technology, Örebro University, Örebro, Sweden
[*] Author to whom any correspondence should be addressed.

E-mail: davood.khodadad@umu.se

Keywords: phase unwrapping, fuzzy, adaptive reliability

Abstract

Pixel reliability assessment in optical phase unwrapping has relied predominantly on deterministic scalar metrics that cannot capture the multi-dimensional nature of phase quality in practical interferometric measurements. We present a multi-input fuzzy inference framework for optical phase unwrapping that introduces linguistic reasoning for pixel reliability assessment. Unlike conventional deterministic approaches that rely on scalar curvature measures, the proposed framework evaluates pixel trustworthiness using three fuzzy variables: phase smoothness, directional isotropy, and local consistency. This approach provides adaptive reliability assessment, a capability that fixed-threshold deterministic methods fundamentally cannot achieve, without the training data demands of deep learning alternatives, while maintaining exact 2π periodicity through graph-based non-continuous propagation. Validation on simulated and experimental data demonstrates equivalent performance to conventional methods under noise-free conditions, with enhanced robustness in challenging scenarios including moderate noise (1.67× RMS improvement) and opposing gradient discontinuities (4.4× improvement). The framework maintains sub-second processing times while offering tunable parameters for application-specific optimization. This fuzzy reliability paradigm introduces adaptive decision-making capabilities to optical phase analysis, particularly beneficial for digital holography and interferometric applications where noise and measurement artifacts are prevalent.

Phase unwrapping is a fundamental challenge in optical interferometry, digital holography, and coherent imaging, requiring reconstruction of continuous absolute phase distributions from wrapped measurements confined to $(-\pi, \pi)$ [1],

The wrapped $\varphi(x,y)$ and absolute continuous $\Phi(x,y)$ phases satisfy:

$$\Phi(x,y) = \varphi(x,y) + 2\pi k(x,y),\ k(x,y) \in Z \tag{1}$$

where $k(x,y)$ denotes an integer phase, rendering the inverse problem inherently ill-posed without additional constraints [2].

Classical unwrapping strategies have evolved along two primary directions: sequential path-following algorithms [3] and path-independent approaches as a global optimization problem [4]. Path-following methods process pixels according to predefined quality or reliability measures, typically derived from local phase characteristics, offering computational efficiency but remaining sensitive to error propagation in noisy regions. In contrast, global approaches formulate phase unwrapping as optimization problems, such as least-squares minimization, providing improved robustness at the expense of higher computational cost. Both paradigms, however, fundamentally rely on deterministic reliability metrics based on local phase gradients, curvature, or scalar quality indices [3, 5, 6].

The fundamental limitation of these deterministic approaches emerges in practical optical measurements, where phase reliability cannot be adequately characterized by single scalar values. Real interferometric data exhibit spatially varying noise characteristics, amplitude modulations, and coherence degradations that require context-sensitive evaluation rather than fixed mathematical thresholds. Investigations

© 2026 The Author(s). Published by IOP Publishing Ltd

have demonstrated that conventional reliability metrics fail to distinguish between genuine phase discontinuities and measurement artifacts, particularly in digital holographic microscopy where fringe contrast varies significantly across the field of view [6, 7]. Recent advances in non-deep-learning approaches, including improved variational regularization and sparse optimization strategies, have partially addressed these challenges [8–10], yet their computational demands and sensitivity to parameter selection remain limiting factors in practical applications.

Contemporary machine learning approaches, particularly deep convolutional networks and Transformer architectures, have demonstrated impressive capabilities in learning complex phase-to-phase mappings from extensive training datasets. These methods excel in pattern recognition and can adapt to diverse phase structures through data-driven optimization. However, deep learning solutions face critical limitations for reliability-guided unwrapping applications: (1) they require substantial computational resources and extensive labeled datasets that may not be available in specialized optical systems, (2) they lack interpretability in reliability assessment decisions, making it difficult to understand why certain pixels are deemed trustworthy, (3) they provide limited control over the balance between noise robustness and phase discontinuity sensitivity, and (4) they may not generalize effectively across different optical setups, wavelengths, or measurement conditions without retraining [11–16].

In contrast, fuzzy logic systems offer distinct advantages for reliability assessment in phase unwrapping. Unlike deep learning approaches that learn implicit feature representations, fuzzy inference enables explicit formulation of reliability criteria through linguistic variables and expert-defined rules. This transparency allows optical engineers to incorporate domain knowledge directly into the decision-making process while maintaining mathematical rigor. Furthermore, fuzzy systems can be tuned and adapted without requiring large training datasets [17], making them more practical for specialized optical applications. The rule-based nature of fuzzy inference also provides interpretable reliability decisions that can be validated against physical understanding of phase measurement principles [18].

Building on these considerations, we propose a multi-input fuzzy reliability framework that integrates three key phase characteristics, local curvature, directional balance, and spatial consistency; through Mamdani-type inference rules. This approach enables adaptive reliability assessment that mimics human expert reasoning while maintaining the computational efficiency of classical unwrapping algorithms. The framework addresses the critical gap between rigid deterministic metrics and computationally intensive learning-based approaches, providing a transparent, tunable, and physically interpretable solution for challenging phase unwrapping scenarios.

The framework comprises four stages: (1) multi-input fuzzy reliability inference, (2) fuzzy-weighted edge prioritization, (3) reliability-guided path propagation, and (4) discrete 2π phase correction.

For a wrapped phase matrix $\varphi(i,j)$ of size $N_x \times Ny$, local reliability is derived from a three-input fuzzy inference system that simultaneously evaluates phase curvature, directional balance, and local consistency through overlapping membership functions and Mamdani-type reasoning rules.

For the first input as phase curvature, second-order phase differences are computed as:

$$\begin{aligned} H(i,j) &= \gamma[\varphi(i-1,j) - \varphi(i,j)] - \gamma[\varphi(i,j) - \varphi(i+1,j)], \\ V(i,j) &= \gamma[\varphi(i,j-1) - \varphi(i,j)] - \gamma[\varphi(i,j) - \varphi(i,j+1)], \\ D_1(i,j) &= \gamma[\varphi(i-1,j-1) - \varphi(i,j)] - \gamma[\varphi(i,j) - \varphi(i+1,j+1)], \\ D_2(i,j) &= \gamma[\varphi(i-1,j+1) - \varphi(i,j)] - \gamma[\varphi(i,j) - \varphi(i+1,j-1)], \end{aligned} \tag{2}$$

where $\gamma(x) = sign(x).mod(|x|, \pi)$ wraps phase differences into $[-\pi, \pi]$.

The total curvature magnitude is:

$$D_{\text{total}}(i,j) = \sqrt{H^2 + V^2 + D_1^2 + D_2^2}. \tag{3}$$

Directional Balance is the second input. To prevent systematic propagation bias, directional consistency is evaluated as:

$$\text{Balance}(i,j) = \frac{\min(|H|, |V|)}{\max(|H|, |V|) + \varepsilon} \tag{4}$$

where values near unity indicate balanced horizontal and vertical curvatures.

Finally, local phase consistency is used as the third input. Local variance within a 3×3 neighborhood quantifies phase smoothness:

$$\text{Variance}(i,j) = \text{Var}[\varphi(i-1:i+1, j-1:j+1)]. \tag{5}$$

Fuzzy membership functions are also consisted of three functions. Each input variable is characterized by overlapping Gaussian membership functions:

Curvature memberships:

$$\begin{aligned}\mu_{\text{curv}}^{\text{low}}(D) &= \exp\left(-\frac{(D_{\text{norm}}-c_1)^2}{\sigma_c^2}\right)\\ \mu_{\text{curv}}^{\text{med}}(D) &= \exp\left(-\frac{(D_{\text{norm}}-c_2)^2}{\sigma_c^2}\right),\\ \mu_{\text{curv}}^{\text{high}}(D) &= \exp\left(-\frac{(D_{\text{norm}}-c_3)^2}{\sigma_c^2}\right),\end{aligned} \tag{6}$$

where $D_{\text{norm}} = D_{\text{total}}/\max(D_{\text{total}})$, c_1, c_2, c_3 are the curvature membership centers and σ_c controls the overlap between curvature membership functions.

Balance memberships:

$$\begin{aligned}\mu_{\text{bal}}^{\text{poor}}(B) &= \exp\left(-\frac{(B-b_1)^2}{\sigma_b^2}\right),\\ \mu_{\text{bal}}^{\text{good}}(B) &= \exp\left(-\frac{(B-b_2)^2}{\sigma_b^2}\right),\end{aligned} \tag{7}$$

where b_1, b_2 are the balance membership centers, and σ_b controls the balance membership function width.

Variance memberships:

$$\begin{aligned}\mu_{\text{var}}^{\text{low}}(V) &= \exp\left(-\frac{(V_{\text{norm}}-v_1)^2}{\sigma_v^2}\right),\\ \mu_{\text{var}}^{\text{high}}(V) &= \exp\left(-\frac{(V_{\text{norm}}-v_2)^2}{\sigma_v^2}\right),\end{aligned} \tag{8}$$

where $V_{\text{norm}} = \text{Variance}/\max(\text{Variance})$, v_1, v_2 are the variance membership centers, and σ_v controls the variance membership function width.

The reliability fuzzy inference system employs four Mamdani-type rules:

- Rule 1: IF curvature *Low* AND balance *Good* AND variance *Low* → reliability *High*
- Rule 2: IF curvature *Medium* AND balance *Good* → reliability *Medium*
- Rule 3: IF balance *Poor* OR variance *High* → reliability *Low*
- IF curvature *High* → reliability *Low*

Rule activation strength are computed as:

$$\begin{aligned}\alpha_1 &= \min\left(\mu_{curv}^{low},\ \mu_{bal}^{good},\ \mu_{var}^{low}\right),\\ \alpha_2 &= \min\left(\mu_{curv}^{med},\ \mu_{bal}^{good}\right),\\ \alpha_3 &= \max\left(\mu_{bal}^{poor},\ \mu_{var}^{high}\right),\\ \alpha_4 &= \mu_{curv}^{high},\end{aligned} \tag{9}$$

These rules implement the principle that high reliability requires simultaneously low curvature, good directional balance, and low local variance (Rule 1), while poor directional balance or high noise immediately reduces reliability regardless of other factors (Rule 3).

Output fuzzy sets are aggregated as:

$$\begin{aligned}\text{out}_{\text{high}} &= \alpha_1,\\ \text{out}_{\text{medium}} &= \alpha_2,\\ \text{out}_{\text{low}} &= \max(\alpha_3, \alpha_4).\end{aligned} \tag{10}$$

The final reliability index is obtained through centroid defuzzification:

$$R(i,j) = \frac{w_h\, out_{\text{high}} + w_m\, out_{\text{medium}} + w_l\, out_{\text{low}}}{out_{\text{high}} + out_{\text{medium}} + out_{\text{low}} + \varepsilon} \tag{11}$$

where w_h, w_m and w_l are the reliability class centroids, yielding $R(i,j) \in [0,1]$.

A final Gaussian smoothing operation ensures spatial continuity of the reliability surface:

$$R_{\text{final}}(i,\, j) = G_{\sigma_S} * R(i,j), \tag{12}$$

where G_{σ_S} is the Gaussian kernel with standard deviation σ_s.

The resulting pixel reliabilities are then used to construct a weighted graph for phase propagation. Each pixel is treated as a node connected to its orthogonal neighbors, with edge weights determined by the fuzzy reliabilities of the connected pixels. Horizontal and vertical edge reliabilities are computed as the arithmetic mean of adjacent pixel reliabilities:

$$\begin{aligned} E_h(i,\, j) &= \frac{R_{\text{final}}(i,j)+R_{\text{final}}(i,j+1)}{2}, \\ E_v(i,\, j) &= \frac{R_{\text{final}}(i,j)+R_{\text{final}}(i+1,j)}{2}. \end{aligned} \tag{13}$$

The complete edge set $E = [E_h(:);\, E_v(:)]$ is sorted in descending reliability order to establish the unwrapping priority sequence. This fuzzy-weighted edge prioritization ensures that the most reliable pixel connections are processed first during the non-continuous path propagation, while discrete 2π phase corrections maintain exact periodicity at each merge operation.

The implemented fuzzy system uses the following parameter values:

- Membership centers: $c_1 = 0$, $c_2 = 0.5$, $c_3 = 1$; $b_1 = 0$, $b_2 = 1$; $v_1 = 0$, $v_2 = 1$
- Membership widths: $\sigma_c = \sigma_v = 0.3$, $\sigma_b = 0.2$
- Output weights: $w_h = 0.9$, $w_m = 0.5$, $w_l = 0.1$
- Spatial smoothing: $\sigma_s = 0.5$ pixels

The membership centers define the phase quality thresholds at which each linguistic category transitions. For curvature and variance, the centers are positioned at the minimum (0), midpoint (0.5 for curvature), and maximum (1) of their respective normalized ranges; directional balance is defined as the ratio of the smaller to the larger directional curvature component, which naturally falls within [0, 1] without requiring explicit normalization, with centers placed at 0 (poor balance) and 1 (good balance). The membership widths σ_c, σ_b, and σ_v control the degree of overlap between adjacent fuzzy categories: narrower widths produce sharper transitions and more selective reliability assessment, while wider values yield smoother, more tolerant classification. The curvature and variance widths ($\sigma_c = \sigma_v = 0.3$) are intentionally broader than the balance width ($\sigma_b = 0.2$), reflecting the greater sensitivity of the unwrapping process to directional imbalance. The output weights $w_h = 0.9$, $w_m = 0.5$, and $w_l = 0.1$ define the centroid positions of the high, medium, and low reliability classes during centroid defuzzification, and were set to reflect a conservative bias toward low reliability in ambiguous regions. The spatial smoothing parameter $\sigma_s = 0.5$ pixels applies mild Gaussian averaging to the reliability surface to suppress isolated outliers while preserving spatial gradients. In practice, applications with high fringe density may benefit from reduced σ_c to sharpen curvature sensitivity, while measurements with inherently low coherence may require wider σ_b to avoid over-penalizing directional imbalance. The values reported here were found to generalize well across all tested scenarios without application-specific tuning.

The proposed fuzzy reliability framework was evaluated using simulated and experimental phase data to assess unwrapping accuracy and noise robustness. Figure 1 demonstrates performance on simulated data: (a) ground truth phase map, (b) corresponding wrapped phase, and (c) 3D surface representation. The selected profile line used for line-profile comparison is indicated in (a). The unwrapped results from the conventional reliability-guided method [6] (d) and the proposed fuzzy framework (e) both achieve perfect reconstruction with zero RMS error, confirming mathematical equivalence under noise-free conditions. The line profile comparison (f), extracted along the profile line indicated in (a), shows identical phase recovery, with execution times of 0.29 s (conventional) and 0.57 s (fuzzy) for the 257 × 257 pixel image.

Figure 2 presents results for experimental interferometric data of a candle flame from the benchmark dataset [11]: (a) absolute phase ground truth, (b) wrapped measurements, and (c) reconstructed temperature distribution obtained from the absolute phase using the temperature reconstruction method described in [19]. The selected profile line used for line-profile comparison is indicated in (c). Both methods successfully unwrap the flame structure, as evidenced by the reconstructed temperature distributions shown in (d) and (e), computed from the phase maps obtained using the conventional

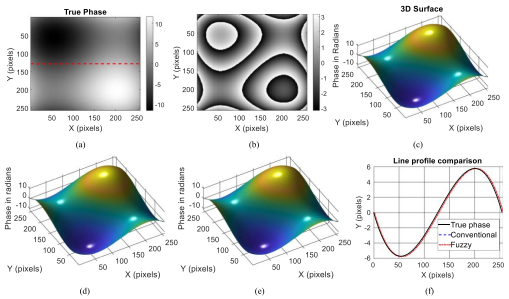

Figure 1. Simulated phase data evaluation: (a) ground truth, (b) wrapped phase, (c) 3D surface, (d) conventional unwrapping, (e) fuzzy framework result, (f) line profile comparison. Both methods achieve perfect reconstruction on noise-free data.

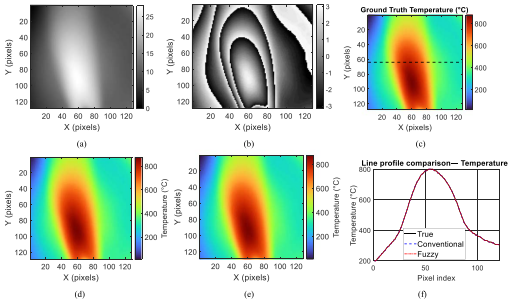

Figure 2. Experimental candle flame data [11]: (a) absolute phase ground truth, (b) wrapped measurements, (c) reference temperature distribution obtained using the method of [19], with the selected profile line indicated, (d) conventional method result, (e) proposed fuzzy framework result, (f) comparison of the line profiles extracted along the line indicated in (c). Both methods yield zero RMS error.

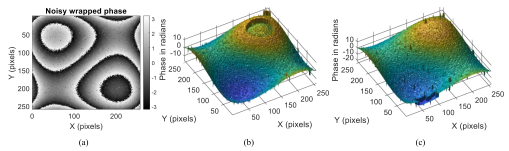

Figure 3. Noise tolerance test ($\sigma = 0.2$ rad, 1% impulse noise): (a) noisy wrapped input, (b) conventional unwrapping with artifacts, (c) fuzzy framework showing improved robustness. RMS errors: 1.63 rad (conventional) vs 0.98 rad (fuzzy).

reliability-guided method and the proposed fuzzy framework, respectively. Both methods yield zero RMS error, with processing times of 0.04 s and 0.11 s, respectively.

To evaluate noise tolerance, controlled degradation was applied to the simulated phase map shown in figure 1(a) with Gaussian noise ($\sigma = 0.2$ radians) and 1% salt-and-pepper impulse noise, representing realistic experimental conditions in digital holography. Figure 3 shows the noisy wrapped phase (a) and comparative unwrapping results. The conventional method (b) exhibits significant unwrapping errors and residual discontinuities, while the fuzzy framework (c) demonstrates superior robustness with minimal artifacts. Quantitative analysis reveals RMS errors of 1.63 radians (conventional) versus 0.98 radians (fuzzy), representing a 1.67× improvement and 4.4 dB SNR enhancement, with processing times of 0.19 s and 0.51 s, respectively.

Phase discontinuities with opposing gradients represent a fundamental challenge in optical phase unwrapping, particularly at material boundaries and structural interfaces where abrupt phase reversals occur [20]. To assess performance under these conditions, we examined a synthetic phase map comprising two adjacent regions with opposing slopes separated by a transverse shear boundary. Figure 4 presents: (a) ground truth phase map with conflicting gradient directions, (b) wrapped phase exhibiting the shear structure, and (c) 3D representation illustrating the sharp phase transition. The selected profile line used for the line-profile comparison is indicated in (a). The conventional method (d) fails catastrophically with numerous false wraps, yielding an RMS error of 24.02 radians. The fuzzy framework (e) successfully reconstructs the phase structure with only minor boundary artifacts, achieving an RMS error of 5.24 radians, a 4.45× improvement over the conventional approach. The line profiles

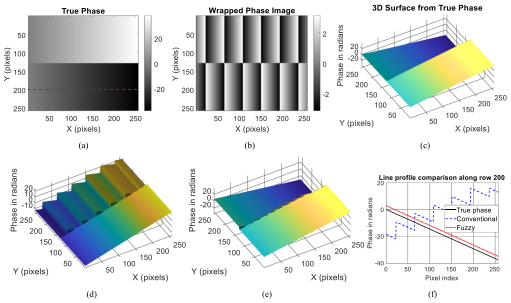

Figure 4. Phase discontinuity challenge with opposing gradients: (a) ground truth, (b) wrapped phase, (c) 3D view, (d) conventional failure, (e) fuzzy success, (f) comparison. The fuzzy approach handles gradient conflicts more effectively.

extracted along the selected profile line indicated in (a) are compared in (f). These residual artifacts arise primarily at the shear boundary where opposing gradient directions create locally ambiguous reliability assignments: pixels situated at the transition between the two slope regions receive intermediate fuzzy reliability scores, causing occasional incorrect propagation decisions during path sorting. This behavior is inherent to any reliability-guided approach operating on ambiguous local evidence, and could be mitigated in future work through refinement of the directional balance membership functions or incorporation of a post-processing residue correction step. Processing times were 0.14 s (conventional) and 0.55 s (fuzzy), demonstrating that the directional balance mechanism's effectiveness in handling conflicting local gradients comes with modest computational overhead.

The computational overhead of the fuzzy framework (2–4× conventional processing time) remains within practical limits for most applications, with absolute times under 1 s for typical image sizes. This modest increase provides substantial robustness gains in challenging measurement conditions while maintaining the efficiency characteristics of reliability-guided unwrapping.

The fuzzy reliability framework provides interpretable, adaptive pixel reliability assessment through linguistic reasoning over three physically motivated inputs, phase curvature, directional balance, and local consistency, replacing rigid scalar metrics with transparent, rule-based inference. It matches conventional methods under noise-free conditions while delivering substantial robustness improvements under noise (1.67×) and opposing gradient discontinuities (4.4×), without requiring training data or sacrificing sub-second processing practicality.

The framework parameters were selected based on established fuzzy logic principles and yielded satisfactory performance across all tested scenarios; systematic optimization for specific interferometric applications was beyond the scope of this work. Nevertheless, the modular architecture, with independently tunable membership function widths, rule weights, and smoothing parameters, enables straightforward adaptation to particular noise profiles or phase structures. This adaptability represents a key advantage over fixed-threshold deterministic methods, offering a transparent and flexible pathway for customized optimization in specialized optical measurement systems.

Several directions remain open for future investigation. Preliminary tests on higher-frequency sinusoidal phase distributions confirmed that the framework maintains accuracy comparable to the conventional method within the reliable operating range of second-order curvature estimation; beyond this range, both reliability-guided methods encounter fundamental sampling limitations inherent to the unwrapping paradigm itself. Characterizing this boundary systematically across varying noise levels and image resolutions represents a natural extension of this work. Regarding computational scalability, to provide initial evidence beyond the 257 × 257 pixel test cases reported in the primary experiments, the framework was evaluated on images of 512 × 512 and 1024 × 1024 pixels using the noise-free simulated phase map of figure 1. Processing times for the conventional and fuzzy methods were 0.51 s and 1.82 s at 512 × 512 pixels, and 2.30 s and 8.25 s at 1024 × 1024 pixels, respectively, with zero RMS error in all cases. The overhead ratio remained approximately 3.6× across both larger resolutions, indicating that the computational complexity of the fuzzy framework scales similarly to the conventional method rather than growing disproportionately with image size. For the 1024 × 1024 noisy case, processing times were 3.17 s (conventional) and 8.28 s (fuzzy), confirming that noise-induced complexity does not substantially alter the scaling behavior. Larger datasets thus remain practical for offline optical metrology workflows, though real-time applications may benefit from future optimization such as vectorized variance computation or parallel edge sorting. Regarding parameter sensitivity, the membership centers

and widths reported in this work were observed to produce consistent results across all tested scenarios, suggesting reasonable robustness to moderate parameter perturbations; however, a formal sensitivity analysis relating parameter variations to unwrapping accuracy metrics remains an important future step, particularly for application-specific optimization. Finally, the framework is expected to be less effective in scenarios involving very low fringe visibility, strong coherence noise, or phase distributions with spatially dense residues, where the three-input fuzzy assessment may not provide sufficient discriminability. These conditions define the applicability boundaries of the current approach and motivate future integration with adaptive preprocessing or hybrid inference strategies.

Data availability statement

The data that support the findings of this study are openly available at the following URL/DOI: https://doi.org/10.6084/m9.figshare.32894807 [21].

Funding

The authors acknowledge the financial support of Kempestiftelserna (www.kempe.com/) under Grant JCSMK24-0156 for this research.

Conflict of interest

The authors declare no conflicts of interest.

ORCID iDs

Davood Khodadad 0000-0003-2960-3094
Satyam Paul 0000-0003-4720-0897

References

[1] Flynn T J 1997 Two-dimensional phase unwrapping with minimum weighted discontinuity *J. Opt. Soc. Am. A* **14** 2692–701
[2] Huntley J 1989 Noise-immune phase unwrapping algorithm *Appl. Opt.* **28** 3268–70
[3] Zhao M, Huang L, Zhang Q, Su X, Asundi A and Kemao Q 2011 Quality-guided phase unwrapping technique: comparison of quality maps and guiding strategies *Appl. Opt.* **50** 6214–24
[4] Huang H Y H, Tian L, Zhang Z, Liu Y, Chen Z and Barbastathis G 2012 Path-independent phase unwrapping using phase gradient and total-variation (TV) denoising *Opt. Express* **20** 14075–89
[5] Ghiglia D C 1998 Two-dimensional phase unwrapping: theory *Algorithms, and Software* (Wiley)
[6] Herráez M A, Burton D R, Lalor M J and Gdeisat M A 2002 Fast two-dimensional phase-unwrapping algorithm based on sorting by reliability following a noncontinuous path *Appl. Opt.* **41** 7437–44
[7] Bioucas-Dias J, Katkovnik V, Astola J and Egiazarian K 2008 Absolute phase estimation: adaptive local denoising and global unwrapping *Appl. Opt.* **47** 5358–69
[8] Chen D, Liu F, Chen X, Wu Y and Zhang R 2026 Phase unwrapping algorithm based on branch-cut placement and minimum-distance weighting *Appl. Opt.* **65** 6504–13
[9] Zuo C *et al* 2018 Phase shifting algorithms for fringe projection profilometry: a review *Opt. Lasers Eng.* **109** 23–59
[10] Li X, Guo J and Liu Z 2025 Robust wavefront sensing method for reflective optical surfaces based on reference light modulation and total variation regularization *Opt. Express* **33** 18042–60
[11] Wang K, Kemao Q, Di J and Zhao J 2022 Deep learning spatial phase unwrapping: a comparative review *Adv. Photon. Nexus* **1** 014001
[12] Ren Z, Xu Z and Lam E Y 2018 Learning-based nonparametric autofocusing for digital holography *Optica* **5** 337–44
[13] Liu Y, Li X, Jin Z, Chen W, Lam E Y, Feng S, Chen Q and Zuo C 2025 Multimodal adaptive temporal phase unwrapping using deep learning and physical priors *APL Photonics* **10** 046104
[14] Gontarz M, Dutta V, Kujawińska M and Krauze W 2023 Phase unwrapping using deep learning in holographic tomography *Opt. Express* **31** 18964–92
[15] Montresor S, Tahon M, Laurent A and Picart P 2020 Computational de-noising based on deep learning for phase data in digital holographic interferometry *APL Photonics* **5** 030802
[16] Wang B, Cao X, Lan M, Wu C and Wang Y 2024 An anti-noise-designed residual phase unwrapping neural network for digital speckle pattern interferometry *Optics* **5** 44–55
[17] Mamdani E H and Assilian S 1975 An experiment in linguistic synthesis with a fuzzy logic controller *Int. J. Man-Mach. Stud.* **7** 1–13

[18] Jang J-S 1993 ANFIS: adaptive-network-based fuzzy inference system *IEEE Trans. Syst. Man Cybern. Syst.* **23** 665–85
[19] Khodadad D, Tayebi B, Saremi A and Paul S 2023 Temperature sensing in space and transparent media: advancements in off-axis digital holography and the temperature coefficient of refractive index *Appl. Sci.* **13** 8423
[20] Khodadad D 2025 Fast and accurate phase unwrapping for complex phase maps *Appl. Opt.* **64** 6910–7
[21] Khodadad D 2026 Optical Phase Unwrapping Toolbox Based on a Fuzzy Reliability Framework (MATLAB). figshare *Software* (https://doi.org/10.6084/m9.figshare.32894807)